RESEARCH MEMORANDUM

FREE-FALL MEASUREMENTS OF THE EFFECTS OF WING-BODY INTERFERENCE ON THE TRANSONIC DRAG CHARACTERISTICS OF SWEPT-WING—SLENDER-BODY CONFIGURATIONS

By Max C. Kurbjun and Jim Rogers Thompson

Langley Aeronautical Laboratory
Langley Field, Va.

NATIONAL ADVISORY COMMITTEE
FOR AERONAUTICS

WASHINGTON
May 28, 1953

E

NATIONAL ADVISORY COMMITTEE FOR AERONAUTICS

RESEARCH MEMORANDUM

FREE-FALL MEASUREMENTS OF THE EFFECTS OF WING-BODY INTERFERENCE ON THE TRANSONIC DRAG CHARACTERISTICS OF SWEPT-WING—SLENDER-BODY CONFIGURATIONS

By Max C. Kurbjun and Jim Rogers Thompson

SUMMARY

In order to provide information on the drag characteristics of airplane configurations and their component parts at transonic speeds the National Advisory Committee for Aeronautics has conducted several series of tests of bodies and wing-body combinations by the free-fall method.

As part of one series, drag measurements were made near zero lift for two wing-body combinations consisting of a fineness-ratio-12 body of revolution having 45° sweptback wings located at different positions on the body. The results, presented in NACA RM L7I01, indicated that a large favorable interference effect on drag occurred when the wing was located behind the maximum body diameter.

In an effort to verify the existence of the favorable interference effect and to obtain more detailed information that might explain its source, two similar models were constructed and dropped. These two models included improved drag measuring instrumentation, and one included pressure measuring orifices on that portion of the body that was expected to be influenced by the presence of the wing. Results of these tests are presented herein.

The tests on these two models failed to confirm the existence of the favorable interference effect. The drag of the body in the presence of the wing was found to be larger (approximately 100 percent at $M = 0.99$ and 18 percent at $M = 1.05$) than that of the body alone. The pressure distribution on the body of the configuration having the wing located behind the maximum body diameter was found to be similar to the distribution on a similar body tested without wings (NACA RM L9J27) but with an additional pressure field similar in shape to that expected at the root of a swept wing superimposed upon it. The principal effect of the additional pressure field was a reduction of the critical Mach number

~~UNCLASSIFIED~~

of the body. The resulting body drag rise occurred in a manner similar to that of the body-alone configuration of NACA RM L9J27 but at a lower Mach number because of the lower critical Mach number of the wing-body combination. Comparison of the results presented herein with previously published results for a similar model having the wing mounted forward of the maximum body diameter showed that the longitudinal position of the wing on the body did not affect the unfavorable drag interference appreciably.

INTRODUCTION

In order to provide information in the transonic speed range (where theory is largely nonexistent) the NACA in 1944 instituted a program of measurements of the drag near zero lift of wing-body combinations and their component parts by the free-fall method. One series of tests was conducted on bodies and wing-body combinations consisting of a body of revolution of fineness ratio 12 and wings of various sweep, aspect ratios, thickness ratios, and taper ratios located at several different positions on the body.

Results are presented in references 1 and 2 for two models of this series which had 45° sweptback constant-chord wings with NACA 65-009 airfoil sections (measured perpendicular to the leading edge) and differed only in the location of the wings on the body. These results indicated that, for the model referred to herein as model B + WA1 (basic body plus wings mounted aft of the maximum diameter, model number 1), the drag rise occurred at a higher Mach number and that the drag at low supersonic speeds was appreciably less than that of model B + WF1 the wing of which was mounted forward of the maximum body diameter. These results, when compared in reference 1 with results for the body without wings, indicated that the difference in drag was due to a favorable interference effect of the wing on the body and that the drag of the body of model B + WA1 was lower than the drag of the body tested without wings.

Additional information on wing-body interference effects has been obtained in free-fall tests of other configurations similar to those discussed herein (wings located behind the maximum body diameter). Interference effects on the body drag are shown in reference 3 which are unfavorable below and favorable above the speed of sound for configurations having 9- or 12-percent-thick untapered wings swept back 35°. However, for configurations having tapered 12-percent-thick wings, either swept back or swept forward 35°, the interference effects were large and unfavorable throughout the Mach number range. Results of tests of a canard configuration derived from model B + WA1 provided some evidence of the presence of a favorable interference effect (ref. 4); however, the

data were obtained only under lifting conditions and extensive calculations were required to estimate the zero-lift drag. Also, results of tests of rocket-powered models having different body shapes (ref. 5) indicated that in the transonic speed range the wing plus wing-body interference drag is reduced by a change in the body shape which places the maximum body diameter forward of the wing and reduces the slope of the afterbody surface. As the wing drag was not measured separately, the results of reference 5 do not indicate whether the interference drag on the body was favorable or unfavorable.

As a means of investigating the flow phenomena producing the favorable interference effect on the body drag indicated by the results of reference 1, pressure and drag measurements were made on two models. The first model (model B) was the basic body without wings and the results obtained are presented in reference 6. The second model (model B + WA2) was similar to model B + WA1, differing only in that it incorporated an airspeed boom and had pressure measuring orifices located on the rear half of the body. The drag and pressure results for this model did not confirm the favorable interference effect found in the previous tests. Subsequently, a model externally similar to model B + WA1 (model B + WA3) but with only drag measuring instrumentation was tested to verify the drag results obtained for model B + WA2.

Presented herein are the results obtained for model B + WA2 (pressure and drag results) and model B + WA3 (drag results only). The drag results are compared to those previously obtained for similar wing-body combinations and their component parts in order to illustrate the nature of wing-body interference effects at transonic speeds and the effects of wing location on these interferences. The pressure-distribution results are compared with those for model B and with the theoretical pressure distribution for the body.

The conclusions of reference 7 which evaluate the transonic drag characteristics of a large wing fillet are reexamined in the light of the results presented herein.

APPARATUS AND METHOD

Test configuration.- Models B + WA2 and B + WA3 are externally similar to model B + WA1 (ref. 1) except that the pressure-distribution model (B + WA2) incorporated a nose boom with provision for the measurement of static and total pressure. The general arrangement, details, and dimensions of the configurations are shown in figure 1. Figure 2 is a photograph of model B + WA3 which is also representative of models B + WA1 and B + WA2. The coordinates of the body surface are given in table I and the coordinates of the wing section are given in table II.

Measurements.- Measurements of the flight path and the quantities velocity, over-all drag, wing drag, and tail drag were accomplished as described in references 1 and 2. The over-all drag was measured by an improved three-step accelerometer that greatly increased the accuracy of the drag parameters (particularly at the lower Mach numbers) over that obtained in the tests of models B + WA1 and B + WF1. Model B + WA3 did not include instrumentation for the measurement of tail drag.

Model B + WA2 contained additional instrumentation which measured the static and the total-head pressures at the nose boom continuously throughout the drop and sampled the pressure at the 18 body orifices (the locations of which are given in table III) approximately three times per second (about twice per 0.01 change in Mach number). The pressure at those orifices was measured with respect to the static pressure at the airspeed boom as described in reference 8. This system has the advantages of providing sufficient accuracy, low lag, and a continuous check on the drift of the telemetering system.

Precision of measurements.- The estimated maximum uncertainty of the telemetered measurements is of the order of ±1 percent of the full range of the instrument and the uncertainty of the Mach number determined from the flight path measurement is less than ±0.01. Based on these values, the estimated maximum uncertainties of the drag parameters determined from acceleration and force measurements are given in table IV. The values for total drag and wing-drag coefficients are referred to the total wing plan area; whereas values for body and tail-drag coefficients are referred to the body frontal area. The estimated maximum uncertainty of the values of the body pressure coefficients are of the order of ±0.026 at a Mach number of 0.95 and ±0.007 at $M = 1.24$.

RESULTS AND DISCUSSION

Pressure Data

The basic pressure data for model B + WA2 in coefficient form are presented as a variation with Mach number in figure 3. In this form details of changes in pressure coefficient throughout the complete test Mach number range are illustrated for each of the orifice locations from which samples were obtained.

For a detailed study of the flow over the body, the basic data of figure 3 are crossplotted in figure 4 in the form of pressure coefficient P against orifice location x/l for several Mach numbers. The fairings shown apply to the 0° orifice plane designated in figure 1 (perpendicular to the plane of the wing). The pressure coefficients

obtained from orifices located in planes other than 0° are included as points to show the radial variation of pressure on the body. The fairing shown may differ slightly from the actual distribution because of the limited number of orifices; it is thought, however, that the faired curves show the salient features of the pressure distribution. In order to illustrate the change in pressure coefficients on the body due to the presence of the wing, the pressure coefficients on the body tested without wings (model B) and the pressure coefficients calculated by theoretical means are included in figure 4. The variations labeled "body alone" were taken from reference 6. The pressure coefficient corresponding to the local sonic velocity (P_{cr}) is also indicated on each part of the figure.

Pressure measurements for model B + WA2 were obtained only on the rear half of the body; however, as the wing is located behind the maximum body diameter, the pressure pattern for the front half of the body may be assumed similar to that shown in figure 4 for the body without wings.

A discrepancy is evident in figure 3(d) in that the pressures in the 0° and 180° planes disagree by an amount larger than the estimated uncertainty of the measurement. No explanation of the difference has been found although it should be noted that this difference occurs in the region of maximum rate of pressure change (see fig. 4). This difference is not believed to be due to angle of attack as the model surfaces were carefully alined at 0° and the static margin was large (center of gravity approximately $1\frac{1}{2}$ chords ahead of the wing mean aerodynamic chord).

Subsonic distribution.- In figures 4(a) and 4(b) the measured distribution at $M = 0.75$ and 0.90 are compared with the measured and theoretical distributions for the body without wings. The pressure distribution of the wing-body configuration is seen to be similar to the pressure distribution of the body-alone configuration with a pressure field similar in shape to that expected at the root of a swept wing superimposed upon the body pressure field.

The interference effect of the wing on the body pressure distribution is limited longitudinally to the region of the wing-body juncture; a rapid return to a normal body-alone pressure distribution forward and aft of this juncture is observed. The interference effect does, however, extend radially around the body; the negative pressure region near the trailing edge of the wing-body juncture extends radially with little variation to the plane 90° to the wing.

No separated wake on the body due to the wing interference existed as the full pressure recovery predicted by the theory for the body-alone configuration was realized. The pressure recovery on the rear of the body agreed well with the theoretical results but was not as great as was obtained by the tests on the body-alone configuration, model B. This discrepancy will be discussed subsequently.

Transition from subsonic to supersonic distribution.- Because of the influence of the wing pressure field on the body the critical region on the body of model B + WA2 was near the trailing edge of the wing-body juncture. Although a local sonic Mach number was attained (see fig. 3(d)) in this region at Mach number 0.92, no appreciable change in pressure distribution was observed until a Mach number of 0.95 was reached. Near this Mach number (see fig. 3(e)) a shock forms near the trailing edge of the wing-body juncture and with further increase in Mach number this shock moves rapidly rearward. It is this rapid rearward movement of the shock with the associated abrupt decrease in pressure over the region of maximum rate of change of cross-sectional area that produces the rapid drag rise of the body. As the configuration approaches sonic velocity the shock continues to move rearward (fig. 3(e) to (h)) until the region where rapid pressure recovery normally exists at subcritical speeds is reached. As the shock reaches this body location it leaves the body surface and stands off the body. Confirmation that the shock stands away from the body surface has been obtained from schlieren photographs of similar configurations taken recently in transonic wind tunnels.

The transition from the subcritical type of pressure distribution to the supersonic type was similar to that observed for the body-alone configuration but, because of the influence of the pressure field of the wing on that of the body, the critical Mach number was lower. Thus, the rearward movement of the shock (which was shown in ref. 6 to be directly associated with the drag rise) occurred at a lower Mach number than for the body-alone configuration and the transition took place over a slightly larger Mach number range.

In the transonic speed range the interference effect of the wing on the body pressure distribution is not limited longitudinally to the wing-body juncture region as in the subsonic speed range but extends slightly aft of this region. Also, a large variation in radial pressure distribution was measured in the region of the trailing edge of the wing-body juncture.

It is apparent from figure 3(a) that a shock passed over the orifices at $\frac{x}{l} = 0.50$ (ahead of the wing) at a flight Mach number of about 0.99. This shock, which did not occur on the body tested without wings, is believed to be the detached wing-root bow-wave which occurs in the local supersonic region of the flow over the body. No explanation has been found for the higher local velocities observed in the plane of the wing compared to those on the plane of symmetry.

Supersonic distribution.- The longitudinal pressure distribution of the wing-body configuration at supersonic Mach numbers was similar to the

theoretical supersonic pressure distributions for the body alone, as predicted by the method of reference 9, but with a pressure field similar in shape to that expected at the root of a swept wing superimposed upon it. The interference effect of the swept wing moves slightly aft of the wing-body juncture with increase in supersonic Mach number but the radial variation of the interference effect becomes less with increase in Mach number. As at transonic speeds a large radial variation in pressure was measured by the orifices near the trailing edge of the wing-body juncture at supersonic Mach numbers.

The pressure recovery on the rear of the subject model agrees with that predicted by theory (see fig. 4(g) to (k)) at supersonic speeds as well as at subsonic speeds thus indicating that no appreciable amount of flow separation occurred. This agreement with theory to some extent confirms the suspicion presented in reference 6 that the level of the distributions there presented was somewhat uncertain. However, the presence of wings on the subject model precluded a definite conclusion concerning the level of the results of reference 6.

Drag Data

The basic drag results for models B + WA2 and B + WA3 are presented in figure 5 as the variation with Mach number of the total drag coefficient obtained from the retardation measurements. The contributions of the components to the total drag (obtained by subtracting the measured wing and tail drags from the total drag and ascribing the remainder to body drag and interference) are also shown in the figure. As previously noted, the tail drag was not measured for model B + WA3 (fig. 5(b)). This simplification was considered justified as the drag of identical tails on several other models have agreed within less than the estimated uncertainty of the measurements. It is evident from figure 5 that the initial drag rise for both complete configurations starts at a Mach number of about 0.90 because of the unswept tail. The drag rise becomes steeper near $M = 0.95$ where the drag rises of both the wing and body begin. The abrupt drag rises of all the components are completed as the speed of sound is reached. The total drag coefficient continues to increase slowly as the Mach number is increased above unity as a result of the continual slow increase in wing drag. The drag of the body and tail are nearly constant above the speed of sound. At supersonic speeds the wing contributes about 40 percent, the body 45 percent, and the tail 15 percent of the total drag.

Comparison of similar models (B + WA1, B + WA2, and B + WA3).- Variations with Mach number of the total and component drag coefficients for models B + WA1, B + WA2, and B + WA3 are compared in figures 6 to 9. These models have 45° sweptback wings located aft of the maximum body diameter and differ externally only in that model B + WA2 was

fitted with an airspeed boom. Results for different configurations (models B + WF1 and B) are also included in figures 6 to 9 and are discussed subsequently.

Examination of figure 6 reveals that the variation of total drag coefficient with Mach number for models B + WA2 and B + WA3 agree closely; the maximum discrepancies are within the estimated maximum uncertainties of the drag and Mach number measurements. The same close agreement between models B + WA2 and B + WA3 is evident in the component drags as shown for the wing in figure 7, the body-tail combination in figure 8, and the body in figure 9. The uncertainties of the latter components are, of course, larger than those of the former because of the manner in which they are computed (i.e., body drag = total drag - wing drag - tail drag). The tail drag of model B + WA2 was used to compute the body drag for model B + WA3. The agreement between models B + WA2 and B + WA3 is believed to be representative of the quality of the results obtainable by the free-fall method using the most refined instrumentation and techniques currently available.

The curves presented in figures 6 to 9 for model B + WA1 are in all cases lower than those for models B + WA2 and B + WA3. The wing and tail drags show a delay in drag rise and lower drags compared with the results for the later models and the total drag data show a somewhat larger delay in the drag rise and considerably lower drag.

Both the total-drag and speed data presented in reference 1 were obtained from the telemetered longitudinal acceleration, the total drag directly and the speed (and flight path) by integration of the variation of acceleration with time (considering the flight path angle and gravitational acceleration). A check on the results thus obtained was made by comparison with the flight path measured by radar and phototheodolite equipment. As pointed out in reference 1, however, partial instrumentation failure occurred in the phototheodolite equipment which reduced the accuracy of the checks. Reevaluation of the data of reference 1 revealed no significant mistakes but it is of interest to note that if the drag variation with Mach number measured for these later models is assumed, the flight path computed for the model of reference 1 is in better agreement with the radar-phototheodolite flight path than that computed from the original data.

Although the available evidence implies that the discrepancy between the drags of models B + WA1 and B + WA2 may have resulted from an unexplained drift and/or sensitivity shift of the telemetered accelerations of model B + WA1, the possibility that the drags were different cannot be eliminated. Different drags might result, for example, from different surface roughness, trim, release, atmospheric conditions, etc. (or combinations thereof). The model surfaces and wing and tail alinements (0°) were carefully checked and maintained before the flights on

which the models were dropped. Damage or deterioration of the surface or alinement might have occurred during the climb or release, however. The atmospheric conditions and the times during which the models were exposed were similar for all models.

Additional confirmation of the internal consistency of the later results can be obtained by use of the pressure and drag data for the body-alone and wing-body combinations. To this end the variation with Mach number of the interference drag on the body (defined as the body drag in the presence of the wing less the drag of the body alone) is plotted in figure 10. Variations are shown for models B + WA1 and B + WA2 obtained from the acceleration and force measurements and for model B + WA2 from integration of the measured body pressure distributions. It is immediately apparent from figure 10 that the results obtained by the two (relatively) independent methods are in substantial agreement for model B + WA2 and that both differ greatly from that obtained for model B + WA1.

It appears from the evidence presented that the results for models B + WA2 and B + WA3 should be considered more reliable than the results for model B + WA1.

Wing-body interference, wing-aft configuration.- In view of the discrepancy between the results of reference 1 and those presented herein, it is necessary to reexamine the conclusions there presented. The wing-body interference characteristics of the configuration may be obtained by comparing results for models B + WA2 and B + WA3 with results for model B, the basic body-tail combination tested without wings. The variation with Mach number of the drag coefficient of the body-tail combination of models B + WA2 and B + WA3 (obtained by subtracting the measured wing drag from the measured total drag) is presented in figure 8. Comparison of these curves with that for model B shows that the drag is higher in the presence of the wing throughout the transition from subcritical to supersonic speeds. Thus, the interference effect on the body drag due to the presence of the wing is unfavorable and reaches a maximum just below the speed of sound. Above the speed of sound, the unfavorable effect decreases with increasing Mach number and is negligible above about $M = 1.15$. The differences between the various curves below the initial drag rise are not considered significant in view of the fact that in this region the measurement uncertainties are, as shown in table IV, large compared with the measured drag (low speed, high altitude). The tail drags of models B and B + WA2, shown in the lower part of figure 8, agree closely; this agreement indicates that there is no interference effect on the tail drag due to the presence of the wing.

The variation with Mach number of the body drag coefficient is presented in figure 9. Because of the equivalence of the tail drags of models B and B + WA2 the trends discussed above are again indicated,

although the effect of the presence of the wing on the drag rise is shown more clearly. The drag rise of the body of model B + WA2 began near $M = 0.95$ where the body shock formed and started its rearward movement (see the section entitled "Pressure Data"). The rapid increase in body drag is concomitant with the rearward movement of the shock and it is apparent that the mechanism of the body drag rise in the presence of the wing is similar to that of the body without wings (described in ref. 6) but occurs at a lower Mach number because of the lower critical Mach number of the wing-body combination in the presence of the wing. Thus, the unfavorable interference effect on the body drag due to the presence of the wing occurs primarily as a result of the lower critical Mach number of the combination, and secondarily as a result of the higher drag associated with the flow pattern about the body after the drag rise. This second part of the interference drag decreases rapidly with increase in supersonic Mach number.

The magnitude of the interference effect of the wing on the body drag shown in figures 9 and 10 reaches a maximum of 0.1 at $M = 0.99$ and decreases rapidly to about 0.03 near $M = 1.05$ (increases of about 100 percent and 18 percent, respectively, of the basic body drag). The interference drag continues to decrease with increase in Mach number, becoming negligible above about $M = 1.15$.

Effect of wing position on wing-body interference.- In reference 1 results obtained for model B + WA1 are compared with those for model B + WF1 (which differed only in that the wing was located forward of rather than behind the maximum body diameter) to show the effect of wing location on the body drag. In order to reexamine this effect, results for model B + WF1 are included in figures 6 to 9 for comparison with the results for models B + WA2 and B + WA3. It is immediately apparent from figures 6 and 7 that the total and wing drags of models B + WF1, B + WA2, and B + WA3 agree generally within less than the estimated maximum uncertainty of the measurements; the only remarkable point being the "bump" in the wing drag of model B + WF1 which appears between Mach numbers of 0.96 and 1.01. This bump is not reflected in the total drag curve and therefore, as may be seen from figures 8 and 9, causes a peculiar dip in the drag curves of the body and body-tail combination. In view of the early state of development (and consequent larger uncertainties) of the telemetering system at the time of the test of model B + WF1 (1946) and the absence of an explanation of the dip in body drag from other considerations, the existence of the bump in wing drag is regarded with some skepticism. Thus, within the uncertainty of the measurements there appears to be no appreciable effect of wing location on wing-body interference, the interference being unfavorable and of the same order of magnitude for both of the wing locations investigated. This result is substantiated by the results of reference 8 which presents drag and pressure data for

a configuration differing from those considered herein only in that the wing is tapered and the midchord point at the wing-fuselage juncture is located 5 inches ahead of the body midpoint compared with 15 inches ahead of and behind it for models B + WF1 and B + WA1, B + WA2, and B + WA3, respectively. Results for this model (model B + WC1) are compared with results for models B + WF1, B, and B + WA2 in figure 11 which shows the variation of body-drag coefficient with Mach number. It is apparent that the unfavorable interference on model B + WC1 (the difference between the body drags for model B + WC1 and model B) at supersonic speeds is greater than that of models B + WF1 and B + WA2 by an amount of the same order as the estimated uncertainty of the measurement. This trend is logical in view of the fact that the wing of model B + WC1 had 9 percent more area than those of models B + WF1 and B + WA2. Also, it was shown in reference 3 that for 12-percent-thick sweptback wings, taper had an unfavorable effect on the body drag. The differences in the body-drag-rise Mach numbers for models B + WF1, B + WA2, and B + WC1 are only slightly greater than the uncertainties of the measurements; however, they fall in logical order with the drag-rise Mach number, increasing as the wing is moved forward on the body. This order is consistent with the drag-rise mechanism presented in the section called "Pressure Data" and the pressure distribution of the body without wings given in reference 6 (also shown in fig. 4). The pressure distribution on the body without wings shows a small increase in local Mach number from the forward wing position to the aft position. Thus, superposition of the wing-root pressure distribution at the aft position should result in a slightly lower critical Mach number (and earlier drag rise) for the combination than would superposition of the same wing-root pressure distribution in the forward position. Wind-tunnel tests on a configuration similar to model B + WC1 were made with the wing in two different positions on the body (ref. 10). The results substantiate the conclusions of the present test that changes in wing locations (within the ranges of the body location tested) on the body do not produce significant changes in the total drag of the configuration.

Effect of wing fillet on wing-body interference.- Drag measurements for a model incorporating a large fillet at the wing-body juncture (model B + WA(F)) were compared with results for model B + WA1 in reference 7 in order to determine the effects of a fillet on wing-body interference effects at transonic speeds. As the results of the present test do not agree with the results of reference 1, the comparison of the wing-aft model and the fillet model is reexamined herein by the use of data from the present test. Model B + WA(F) differed from models B + WA1, B + WA2, and B + WA3 only in that a fillet of circular-arc plan form was fitted tangent to the wing leading edge 15 inches outboard of the body and tangent to the body surface at a point 10.5 inches ahead of the original wing-leading-edge—body juncture. The section of the fillet was faired from the basic wing section (NACA 65-009 perpendicular to the wing leading

edge) to an NACA 63-009 section in the plane of the body surface. The trailing edge of the wing was unchanged. The fillet added 7.3 percent to the total frontal area of the model and 4.7 percent to the exposed wing plan area. Model B + WA(F) also incorporated an airspeed boom identical with that of model B + WA2. The variation with Mach number of the total drag coefficient for model B + WA(F) is compared with that for model B + WA2 in figure 12 and it is evident that the curves differ only in minor details. It should be noted that both curves are based on the same wing area (that not including the area of the fillet), and the average increase in drag above the speed of sound (although of the same order as the sum of the estimated uncertainties) is about the same as the increase in area due to the fillet. Thus, it is concluded that the fillet does not appreciably affect the wing-body interference characteristics of the configuration investigated and thus could be used to provide either a stronger wing structure or volume for fuel storage without incurring an excessive drag penalty.

Comparison of results with "axial distribution of cross-sectional area" concept.- Results are presented in reference 11 which indicate that the transonic drag-rise characteristics of thin, low-aspect-ratio wing—slender-body combinations at zero lift are principally dependent on the axial distribution of cross-sectional area normal to the air stream. Thus, the concept implies that the drag-rise characteristics of a wing-body combination should be similar to that of a body of revolution having the same axial variation of cross-sectional area. In order to examine the results presented herein in the light of this concept, the shapes of bodies of revolution having the same axial variation of cross-sectional area as models B + WA1, B + WA2, and B + WA3, B + WF1, and B + WA(F) are compared in figure 13 with the basic body shape (model B).

It is apparent that the effect of the wing in the forward position is to add a rather abrupt "bump" to the center of the body with an appreciable increase in maximum area and that the wing in the aft position increases the maximum area a smaller amount over that of the basic body but increases the slope of the rear of the body appreciably. Inasmuch as it has been shown (refs. 6, 12, and 13), that the initial part of the transonic drag rise occurs principally on the rear portion of the body (reduction of fineness ratio of the rear part of the body corresponding to more abrupt initial drag rises), it would be expected that the drag of the wing-aft configurations would rise more abruptly than that of the wing-forward configuration. However, a compensating effect on the drag of the wing-aft configuration (which would be estimated to be of considerably smaller magnitude) would be present because of its smaller maximum cross-sectional area compared to that of the wing-forward configuration. The secondary part of the drag rise, that occurring on the nose of the body and the effect of the nose on the drag of the tail, would be expected to reduce the difference between the drags of the two configurations as the Mach number is increased beyond that at which the initial part of the drag rise occurs.

Thus, it appears that strict application of the "area rule" concept to the subject configurations would indicate that the wing-aft configuration might be expected to have a somewhat larger initial drag rise than the wing-forward configuration. The experimental data presented in figures 6 and 12 show, however, that within relatively close limits (the same order as the uncertainties of the measurements) the drag rises of the configurations are the same. In the absence of experimental data for the body shapes shown in figure 13, evaluation of the "area rule" in the light of the subject results must of necessity be qualitative. A possible explanation of the discrepancy, however, is the effect of wing taper shown in the results presented in reference 11. Good correlation was there shown between the drag rise of pointed-wing—slender-body configurations and their "equivalent" bodies but discrepancies of the order of 20 percent were shown for a wing having a taper ratio of 0.6. The wings of the subject models are untapered. Highly tapered wings, which have the principal part of their axial distribution of cross-sectional area located near the body center line, obviously more nearly fulfill the slender-body restriction of reference 11 than untapered wings which have an appreciable part of their cross-sectional area located much farther away from the body center line.

CONCLUDING REMARKS

Drag and pressure-distribution measurements have been made by the free-fall method for two wing-body combinations consisting of a body of fineness ratio 12 and a 45° sweptback wing located behind the maximum diameter of the body. The measurements were made to investigate a favorable interference effect on drag found in a previous test of a similar configuration. The interference effect on the body drag due to the presence of the wing was found to be unfavorable. Thus, the results do not confirm the previous result (presented in NACA RM L7I01) which indicated a favorable interference effect to be present. The results presented herein are considered to be the more reliable.

The pressure distribution measured on the body of the wing-body combination was similar to that measured on the body without wings with an additional pressure distribution similar to that expected at the root of a swept wing superimposed upon it. As the wing was located in a region of small body slope, the additional pressure distribution did not affect the drag directly, but reduced the critical Mach number of the body. The drag rise occurred in the same manner described in NACA RM L9J27 for the body without wings but at a lower Mach number because of the lower critical Mach number of the wing-body combination compared with that of the body without wings. The drag of the body in the presence of the wing was greatly increased (about 100 percent at $M = 0.99$) at Mach numbers during and after the drag rise of the wing-body combination but before

the drag rise of the body without wings. After the drag rise of the body without wings, the drag of the body of the wing-body combination was still somewhat higher than that of the body without wings (about 18 percent at $M = 1.05$) and decreased slowly with increase in Mach number. The interference effect became negligible at a Mach number of about 1.15.

Comparison of results for the configurations reported herein which had the wings located behind the maximum body diameter with results previously reported for similar configurations having other wing locations indicated that there was no large effect of wing position on the unfavorable wing-body interference drag for the configurations investigated.

Reexamination of the conclusion presented in NACA RM L8F08 - that use of a large wing fillet results in a large drag penalty at transonic speeds - indicated that the conclusion should be revised. It was found upon comparison with results of the present test that a fillet of the type investigated produced no significant change in the transonic drag characteristics for the wing-body combination.

Langley Aeronautical Laboratory,
National Advisory Committee for Aeronautics,
Langley Field, Va.

REFERENCES

1. Mathews, Charles W., and Thompson, Jim Rogers: Comparison of the Transonic Drag Characteristics of Two Wing-Body Combinations Differing Only in the Location of the 45° Sweptback Wing. NACA RM L7I01, 1947.

2. Mathews, Charles W., and Thompson, Jim Rogers: Free-Fall Measurements at Transonic Velocities of the Drag of a Wing-Body Configuration Consisting of a 45° Swept-Back Wing Mounted Forward of the Maximum Diameter on a Body of Fineness Ratio 12. NACA RM L6L26, 1947.

3. Thompson, Jim Rogers, and Mathews, Charles W.: Effect of Wing Sweep, Taper, and Thickness Ratio on the Transonic Drag Characteristics of Wing-Body Combinations. NACA RM L8K01, 1948.

4. Kraft, Christopher C., Jr., and Mathews, Charles W.: Determination by the Free-Fall Method of the Drag and Longitudinal Stability and Control Characteristics of a Canard Model at Transonic Speeds. NACA RM L50D04, 1950.

5. Morrow, John D., and Nelson, Robert L.: Large-Scale Flight Measurements of Zero-Lift Drag of 10 Wing-Body Configurations at Mach Numbers From 0.8 to 1.6. NACA RM L52D18a, 1953.

6. Thompson, Jim Rogers: Measurements of the Drag and Pressure Distribution on a Body of Revolution Throughout Transition From Subsonic to Supersonic Speeds. NACA RM L9J27, 1950.

7. Cheatham, Donald C., and Kurbjun, Max C.: Transonic Drag Characteristics of a Wing-Body Combination Showing the Effect of a Large Wing Fillet. NACA RM L8F08, 1948.

8. Kurbjun, Max C., and Thompson, Jim Rogers: Transonic Drag Characteristics and Pressure Distribution on the Body of a Wing-Body Combination Consisting of a Body of Revolution of Fineness Ratio 12 and a Wing Having Sweepback of 45°, Aspect Ratio 4, Taper Ratio 0.6, and NACA 65A006 Airfoil Sections. NACA RM L52B12, 1952.

9. Thompson, Jim Rogers: A Rapid Graphical Method for Computing the Pressure Distribution at Supersonic Speeds on a Slender Arbitrary Body of Revolution. NACA TN 1768, 1949.

10. Hallissy, Joseph M., and Bowman, Donald R.: Transonic Characteristics of a 45° Sweptback Wing-Fuselage Combination. Effect of Longitudinal Wing Position and Division of Wing and Fuselage Forces and Moments. NACA RM L52K04, 1953.

11. Whitcomb, Richard T.: A Study of the Zero-Lift Drag-Rise Characteristics of Wing-Body Combinations Near the Speed of Sound. NACA RM L52H08, 1952.

12. Thompson, Jim Rogers, and Kurbjun, Max C.: Drag Measurements at Transonic Speeds of Two Bodies of Fineness Ratio 9 With Different Locations of Maximum Body Diameter. NACA RM L8A28b, 1948.

13. Johnston, J. Ford, and Lopatoff, Mitchell: Study by NACA Wing-Flow Method of Transonic Drag Characteristics of a Blunt-Nose Body of Revolution and Comparison With Results for a Sharp-Nose Body. NACA RM L9C11, 1949.

TABLE I

COORDINATES OF FINENESS-RATIO-12 BODY

[Nose radius, 0.060 in.]

x, in.	y, in.	x, in.	y, in.
0	0	48.00	4.876
.60	.277	54.00	4.971
.90	.358	60.00	5.000
1.50	.514	66.00	4.955
3.00	.866	72.00	4.828
6.00	1.446	78.00	4.610
9.00	1.936	84.00	4.274
12.00	2.365	90.00	3.754
18.00	3.112	96.00	3.031
24.00	3.708	102.00	2.222
30.00	4.158	108.00	1.350
36.00	4.489	114.00	.526
42.00	4.719	120.00	0

TABLE II

WING-SECTION COORDINATES, NACA 65-009 SECTION

[Wing-section coordinates are in inches and are measured perpendicular to the leading edge]

x	y	x	y
0	0	4.80	0.540
.06	.083	5.40	.537
.09	.102	6.00	.520
.15	.127	6.60	.490
.30	.171	7.20	.448
.60	.235	7.80	.398
.90	.286	8.40	.342
1.20	.328	9.00	.280
1.80	.396	9.60	.216
2.40	.447	10.20	.151
3.00	.486	10.80	.088
3.60	.512	11.40	.033
4.20	.531	12.00	.000
Leading-edge radius 0.066			

TABLE III

LOCATION OF ORIFICES ON BODY OF MODEL B + WA2

[Juncture of wing leading edge and body surface at $\frac{x}{l} = 0.554$; juncture of wing trailing edge and body surface at $\frac{x}{l} = 0.696$]

Fraction of body length from nose, x/l	Distance from nose, in.	Radial displacement, deg (wing located in 90°, 270° plane)
0.50	60.0	0°, 90°
.592	71.0	0°
.642	77.0	0°
.683	82.0	0°, 45°, 180°
.733	88.0	0°, 45°
.758	91.0	0°, 45°, 90°, 270°
.833	100.0	0°, 45°, 90°
.862	103.5	0°
.902	108.3	0°
Orifice diameter is $\frac{3}{32}$ -inch		

TABLE IV

ESTIMATED MAXIMUM UNCERTAINTY OF DRAG PARAMETERS

[Drag coefficients C_D are based on the total wing-plan area; drag coefficients C_{D_f} are based on body frontal area]

Model B + WA2

Drag parameter	Mach number			
	0.80	0.95	1.05	1.24
C_D total	±0.0010	±0.0007	±0.0009	±0.0007
C_D wing	±.0012	±.0007	±.0006	±.0004
C_{D_f} tail	±.007	±.005	±.004	±.002
C_{D_f} body	±.036	±.020	±.017	±.009

Model B + WA3

Drag parameter	Mach number			
	0.80	0.95	1.05	1.20
C_D total	±0.0011	±0.0007	±0.0006	±0.0007
C_D wing	±.0014	±.007	±.0006	±.0004
C_{D_f} body and tail	±.034	±.018	±.012	±.010

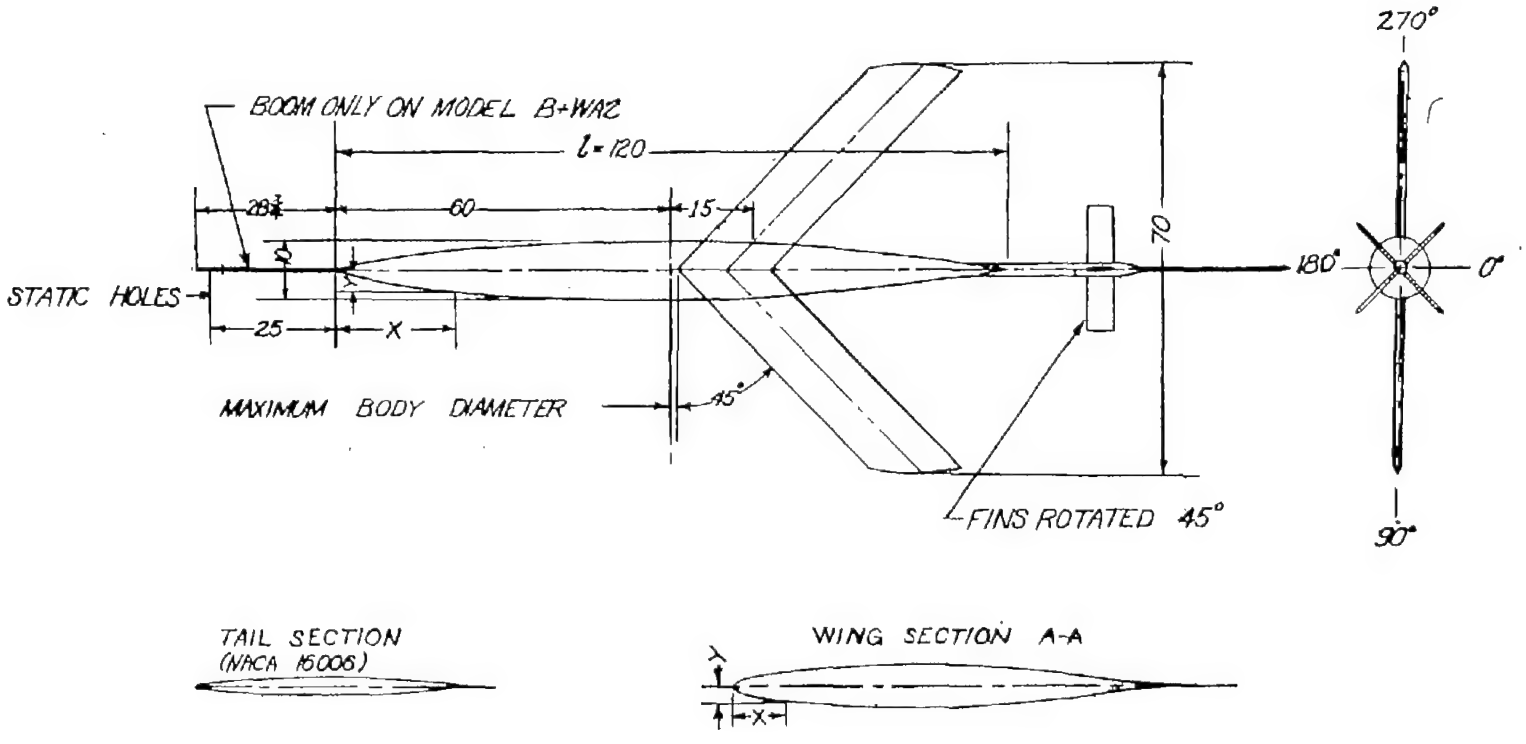

DIMENSIONS Sq.FT.			
BODY FRONTAL AREA	0.545	TOTAL WING PLAN AREA	8.160
WING FRONTAL AREA	.438	TAIL PLAN AREA	1.232
TAIL FRONTAL AREA	.074	TOTAL FRONTAL AREA	1.057

NACA

Figure 1.- Details and dimensions of models tested. Dimensions are in inches unless otherwise specified. Coordinates of the body surface and wing section are given in tables I and II, respectively. The location of pressure orifices (model B + WA2 only) are given in table III.

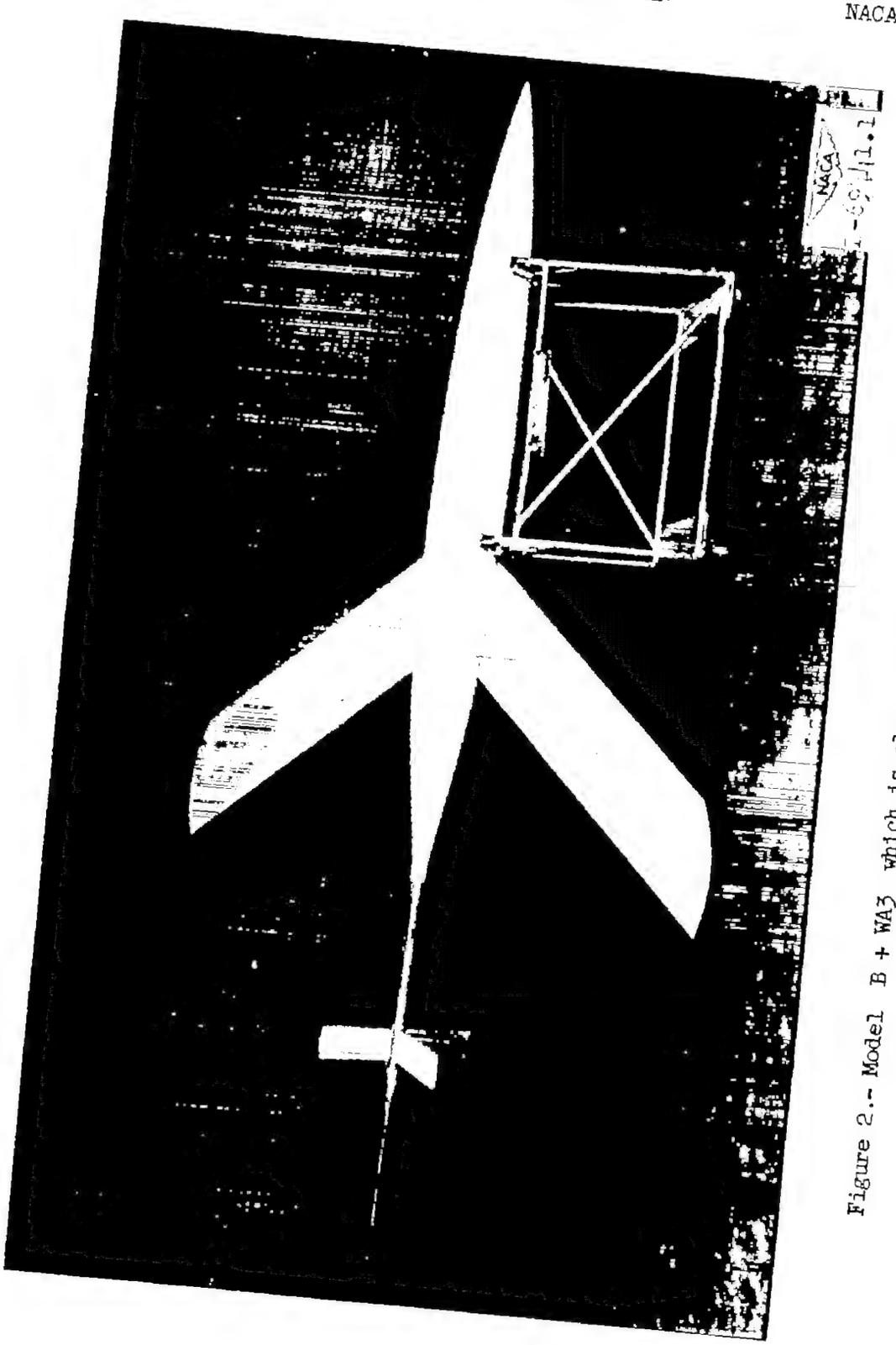

Figure 2.- Model B + WA3 which is also representative of models B + WA1 and B + WA2.

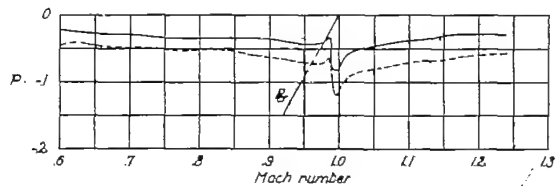

(a) $\frac{x}{l} = 0.50$. 0° ————, 90° - - - - -

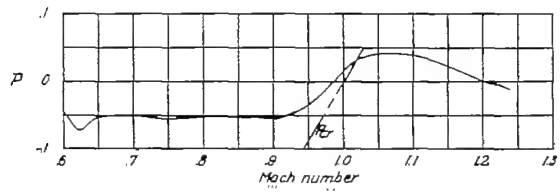

(b) $\frac{x}{l} = 0.592$. 0° ————

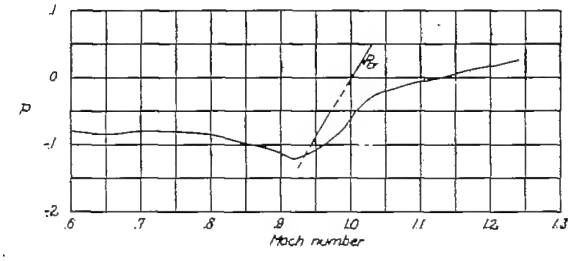

(c) $\frac{x}{l} = 0.642$. 0° ————

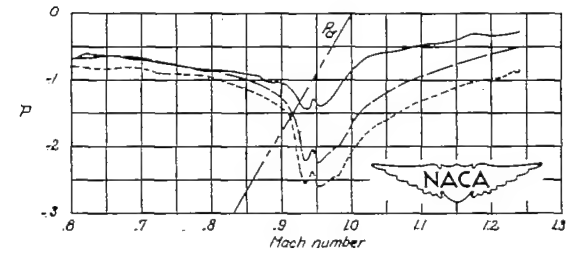

(d) $\frac{x}{l} = 0.683$. 0° ————, 45° - - - - -, 180° —— ——

Figure 3.- The variation with Mach number of the pressure coefficient P measured at each orifice. Lines corresponding to the local speed of sound P_{cr} are also shown. The juncture with the body surface of the wing leading and trailing edges are at $\frac{x}{l} = 0.554$ and $\frac{x}{l} = 0.696$, respectively.

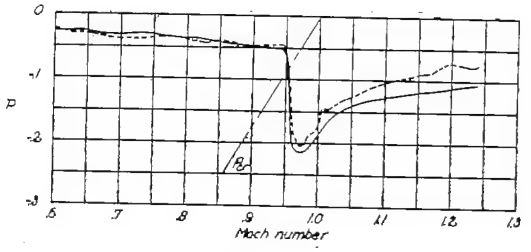

(e) $\frac{x}{l} = 0.733$. 0° ————, 45° - - - - -

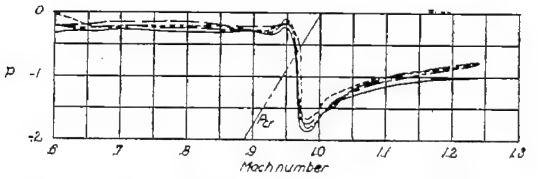

(f) $\frac{x}{l} = 0.758$. 0° ————, 45° - - - - -, 90° —— ——, 270° —— - ——

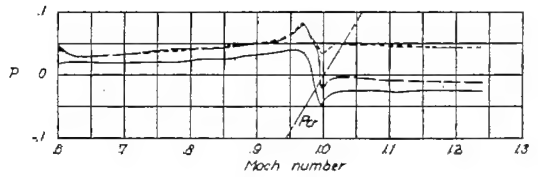

(g) $\frac{x}{l} = 0.833$. 0° ————, 45° - - - - -, 90° —— ——

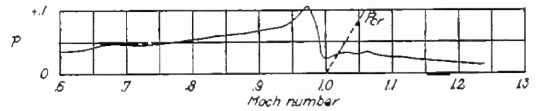

(h) $\frac{x}{l} = 0.862$. 0° ————

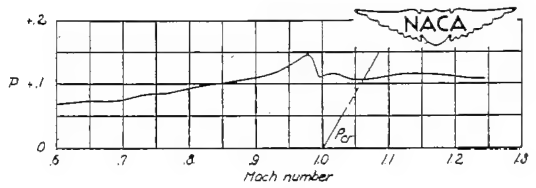

(i) $\frac{x}{l} = 0.902$. 0° ————

Figure 3.- Concluded.

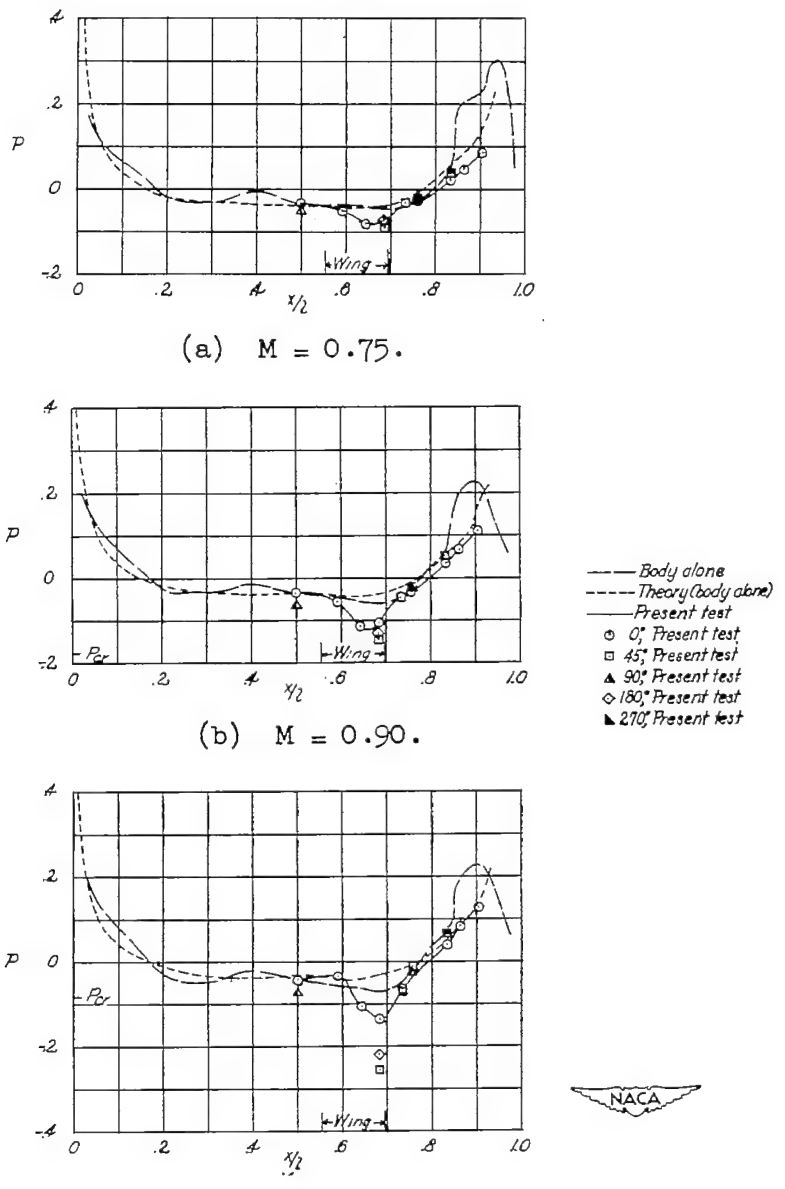

(a) M = 0.75.

(b) M = 0.90.

(c) M = 0.95.

Figure 4.- Variation of pressure coefficient P with orifice location expressed as a fraction of body length x/l for several Mach numbers. Experimental and theoretical distributions for a similar body without wings (taken from ref. 6) are included for comparison. P_{cr} is the pressure coefficient corresponding to the local speed of sound. The wing location indicated is that of the wing-body juncture.

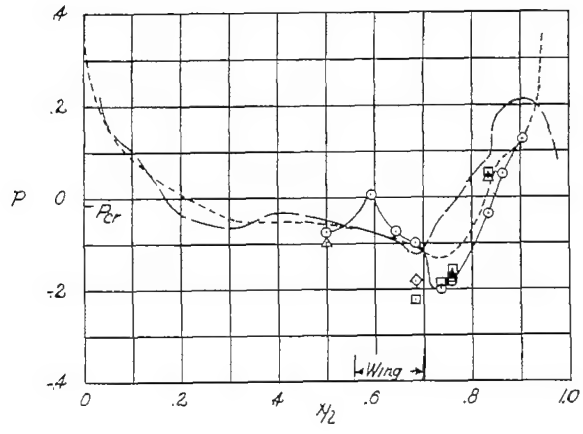

(d) M = 0.99.

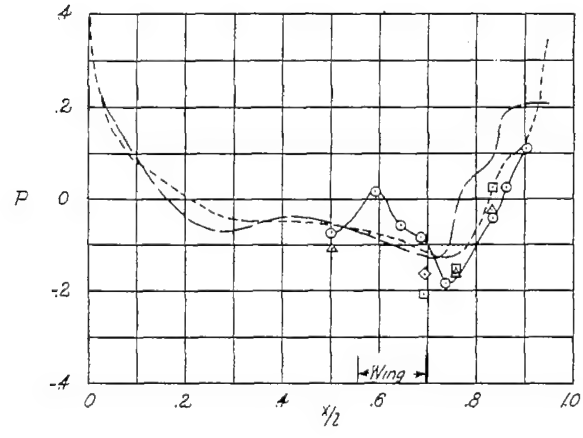

(e) M = 1.00.

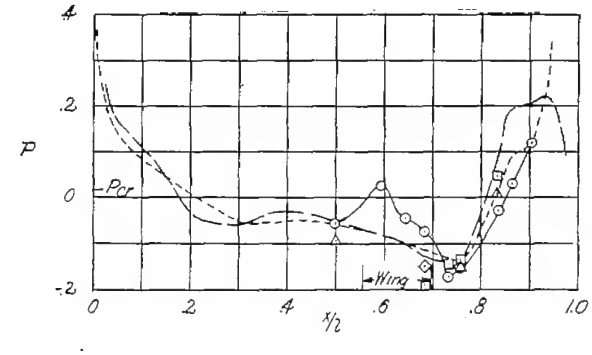

(f) M = 1.01.

Figure 4.- Continued.

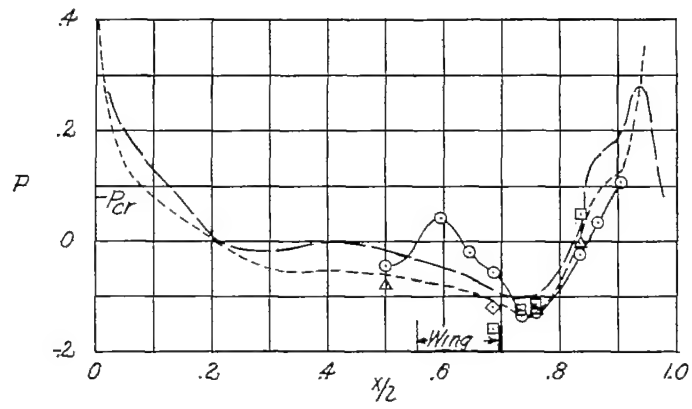

(g) M = 1.05.

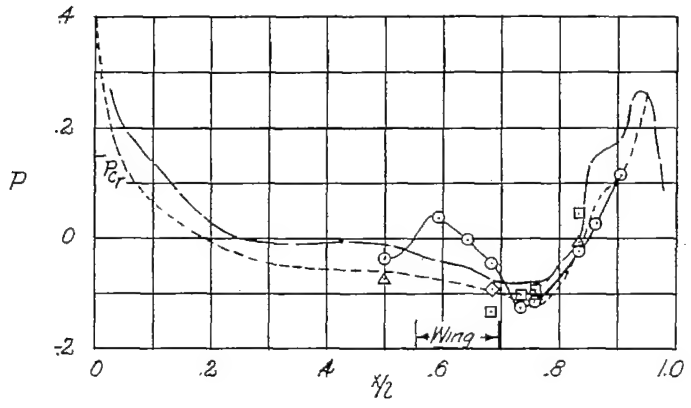

(h) M = 1.10.

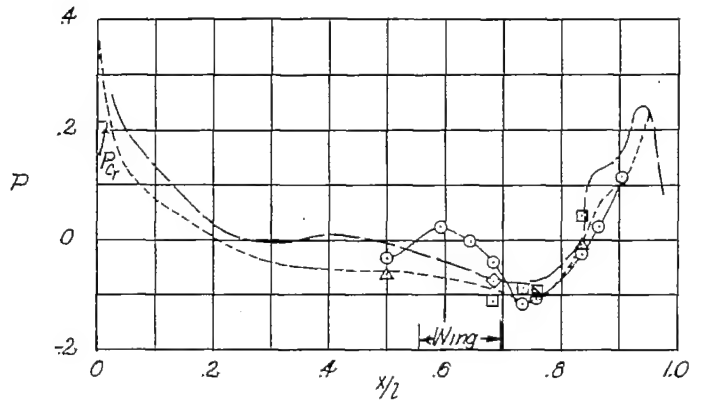

(i) M = 1.15.

Figure 4.- Continued.

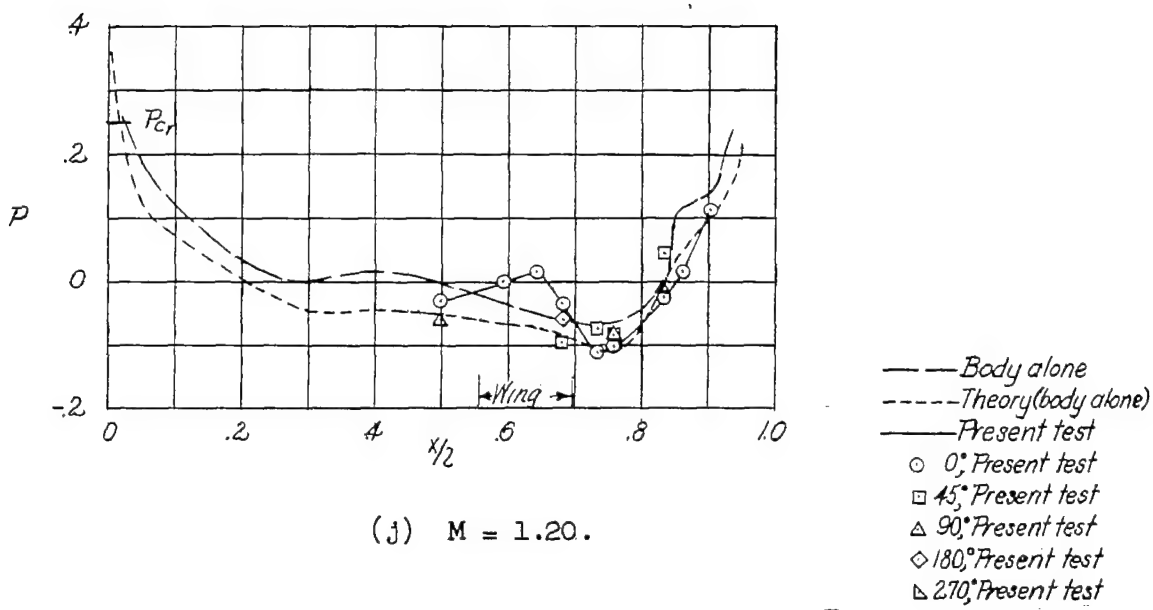

(j) M = 1.20.

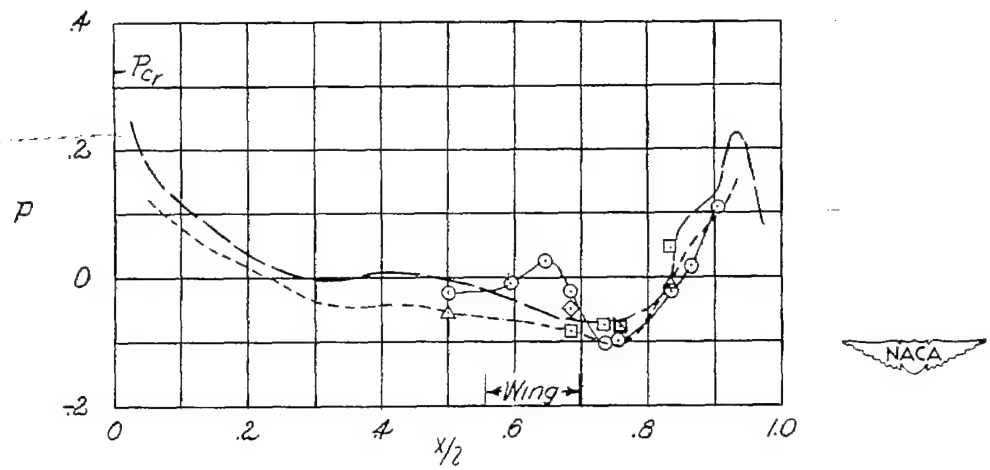

(k) M = 1.24.

Figure 4.- Concluded.

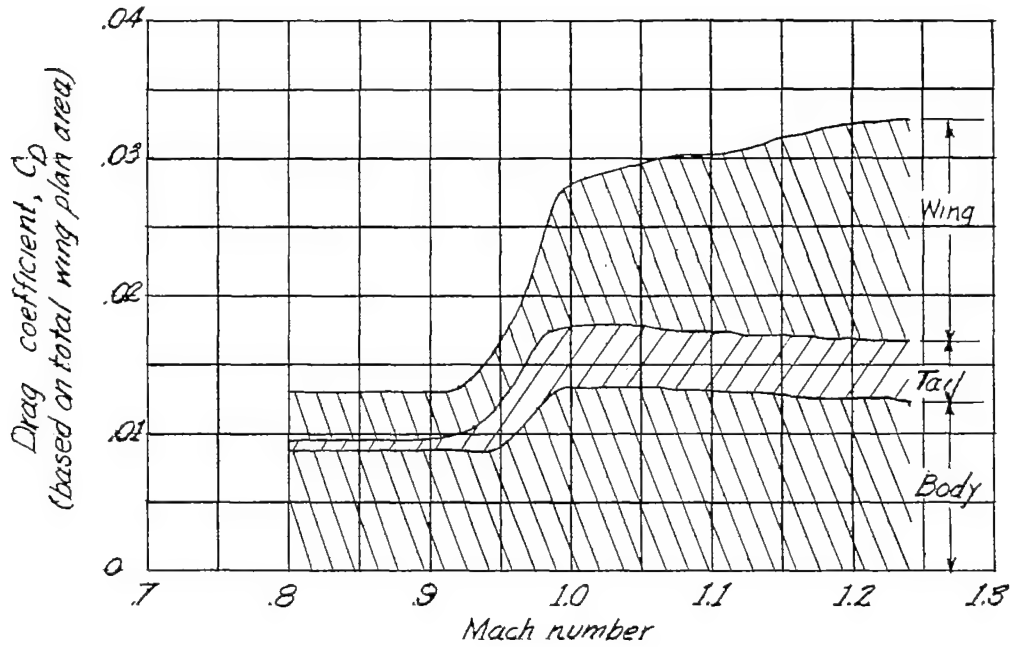

(a) Model B + WA2.

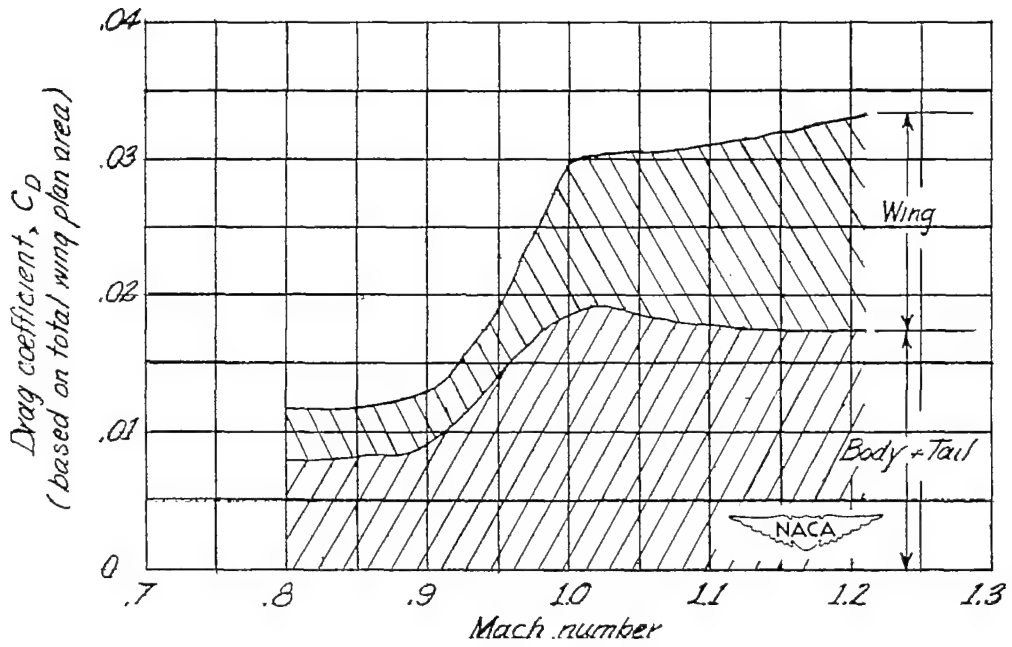

(b) Model B + WA3.

Figure 5.- Variation with Mach number of total drag coefficient for models B + WA2 and B + WA3 showing the division of drag among the component parts.

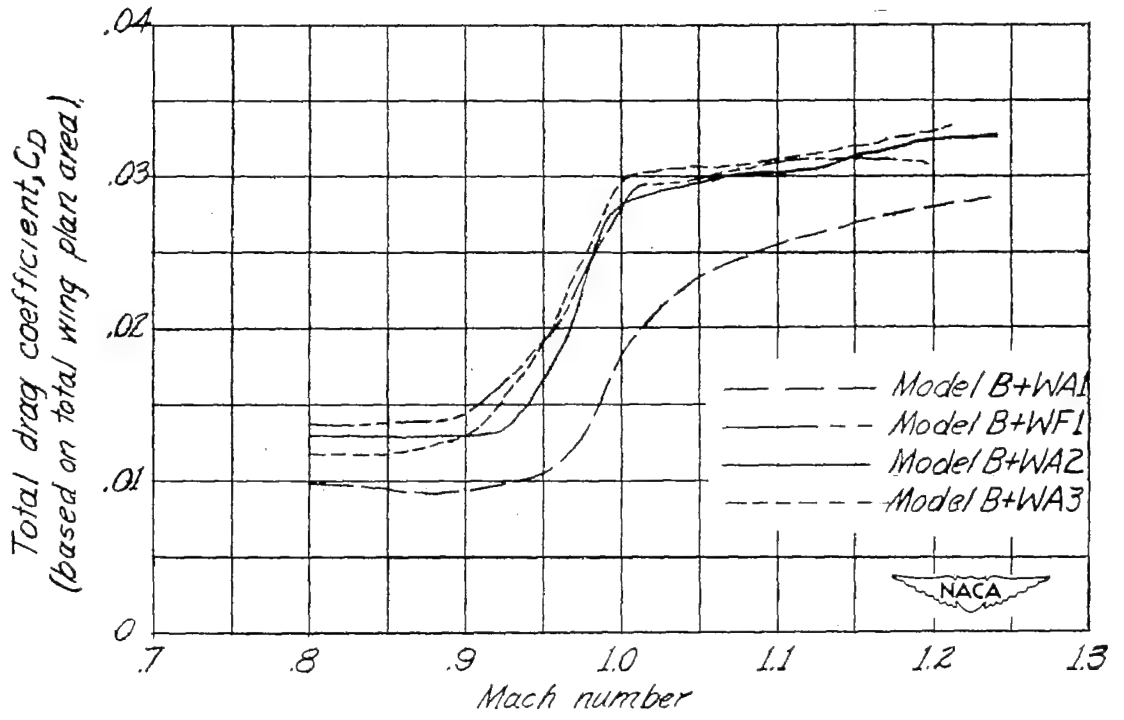

Figure 6.- Comparison of results for models B + WA2 and B + WA3 with results for similar models tested previously. Variation of total drag coefficient with Mach number.

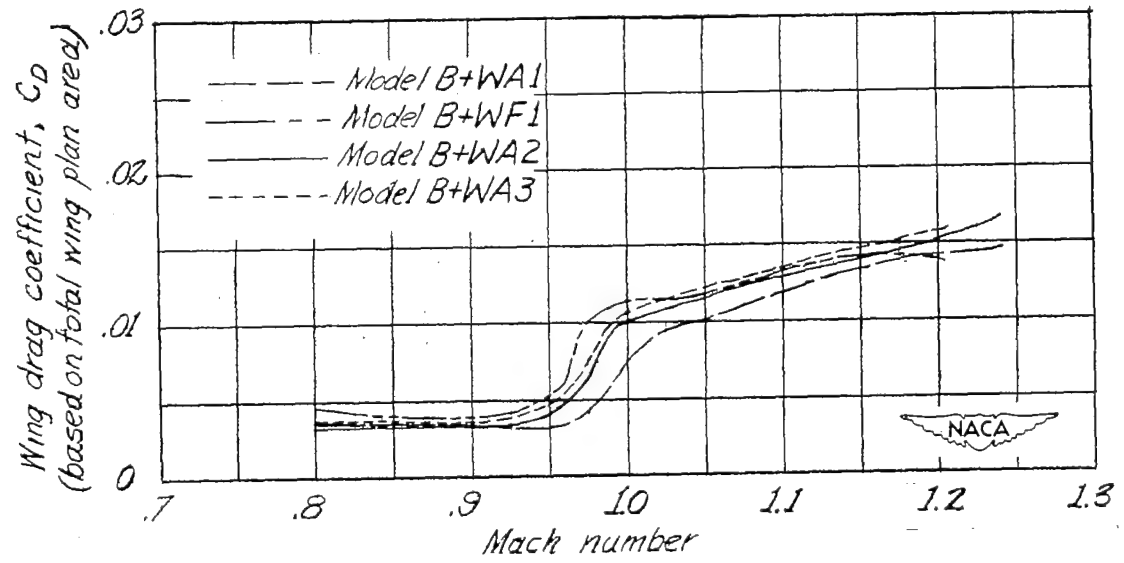

Figure 7.- Comparison of results for models B + WA2 and B + WA3 with results for similar models tested previously. Variation of wing drag coefficient with Mach number.

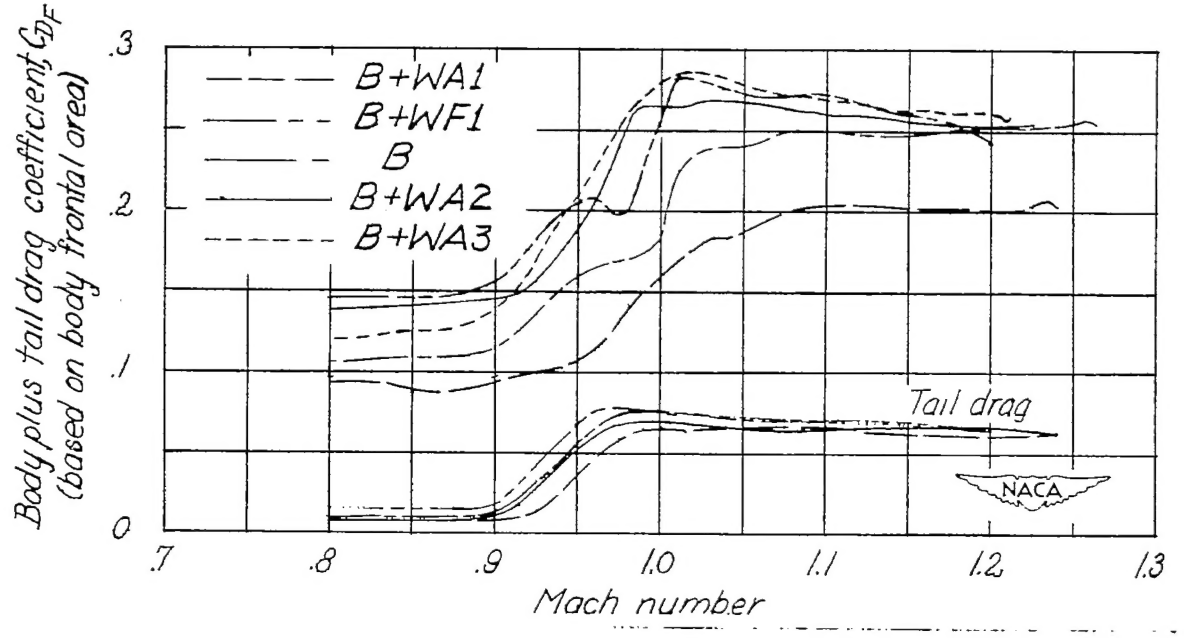

Figure 8.- Comparison of results for models B + WA2 and B + WA3 with results for similar models tested previously. Variation with Mach number of the drag coefficient of the body-tail combination.

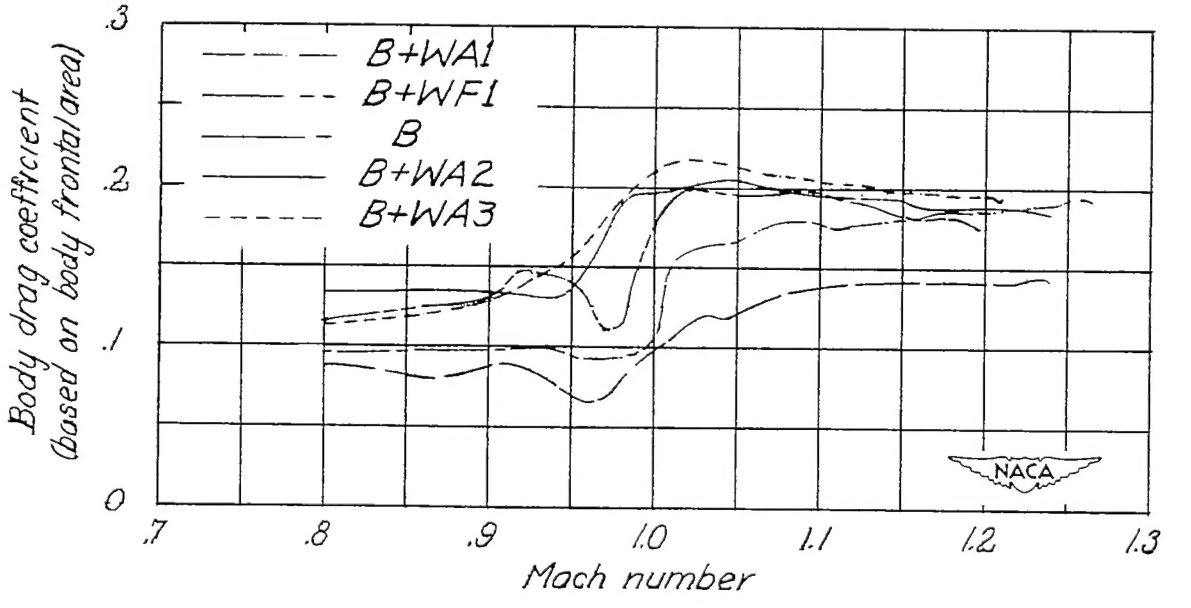

Figure 9.- Comparison of results for models B + WA2 and B + WA3 with results for similar models tested previously. Variation of body drag coefficient with Mach number.

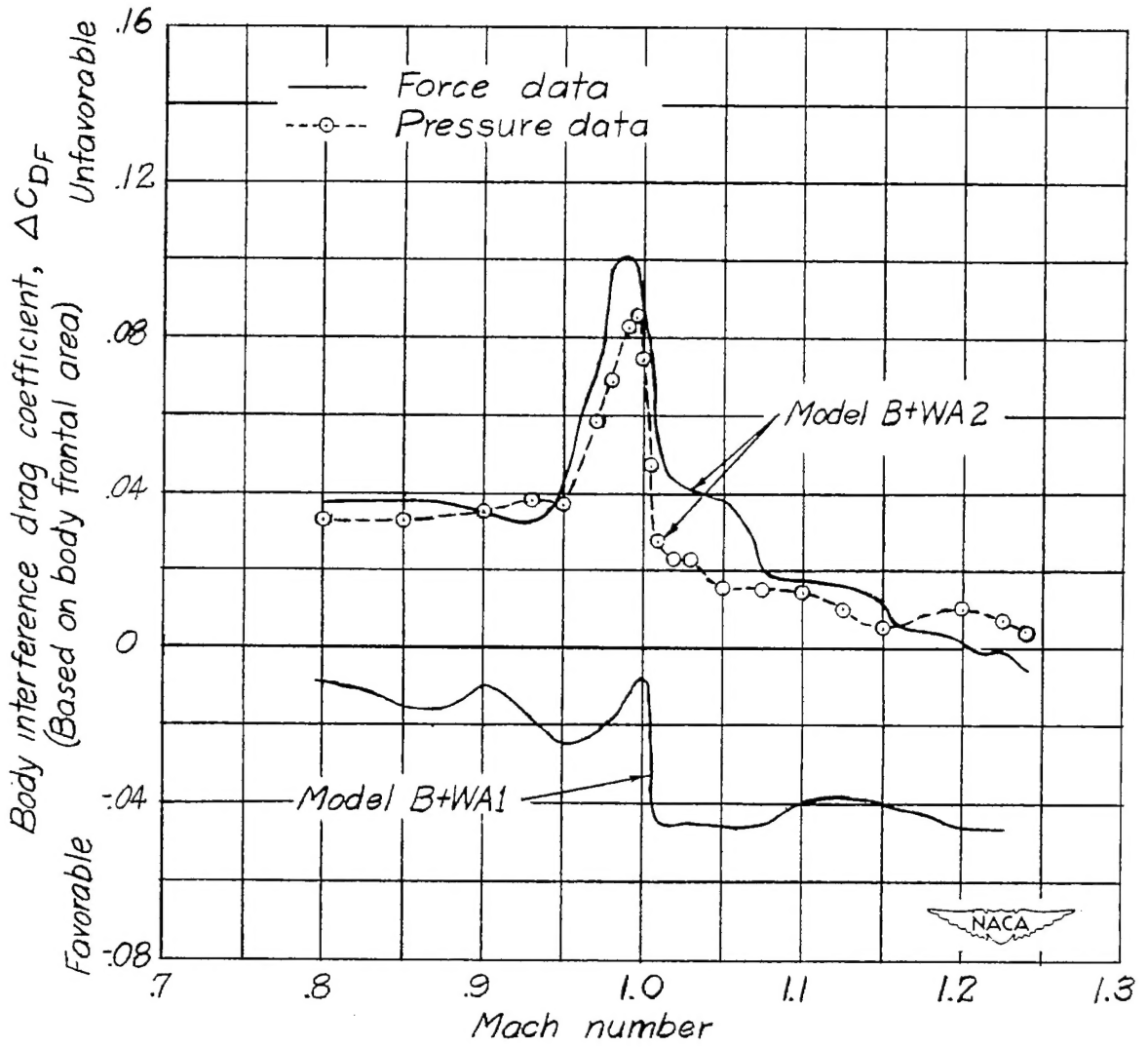

Figure 10.- Variation of Mach number of the body interference drag coefficient for model B + WA2 obtained from two independent measurements. Data for model B + WA1 is included for comparison.

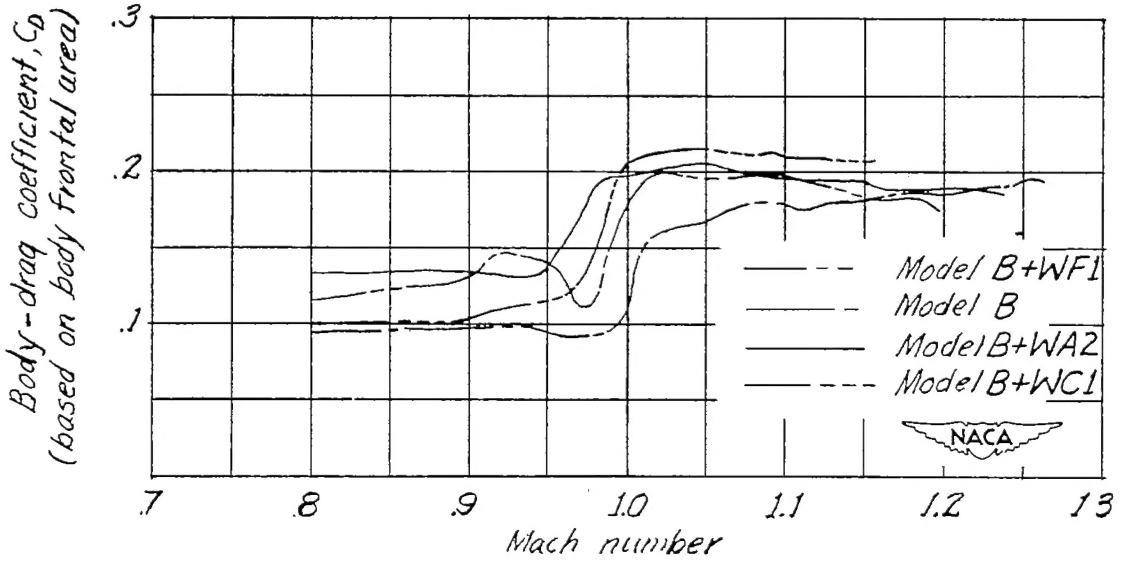

Figure 11.- Comparison of variations with Mach number of body drag coefficient for several configurations illustrating the effect of wing position on wing-body interference.

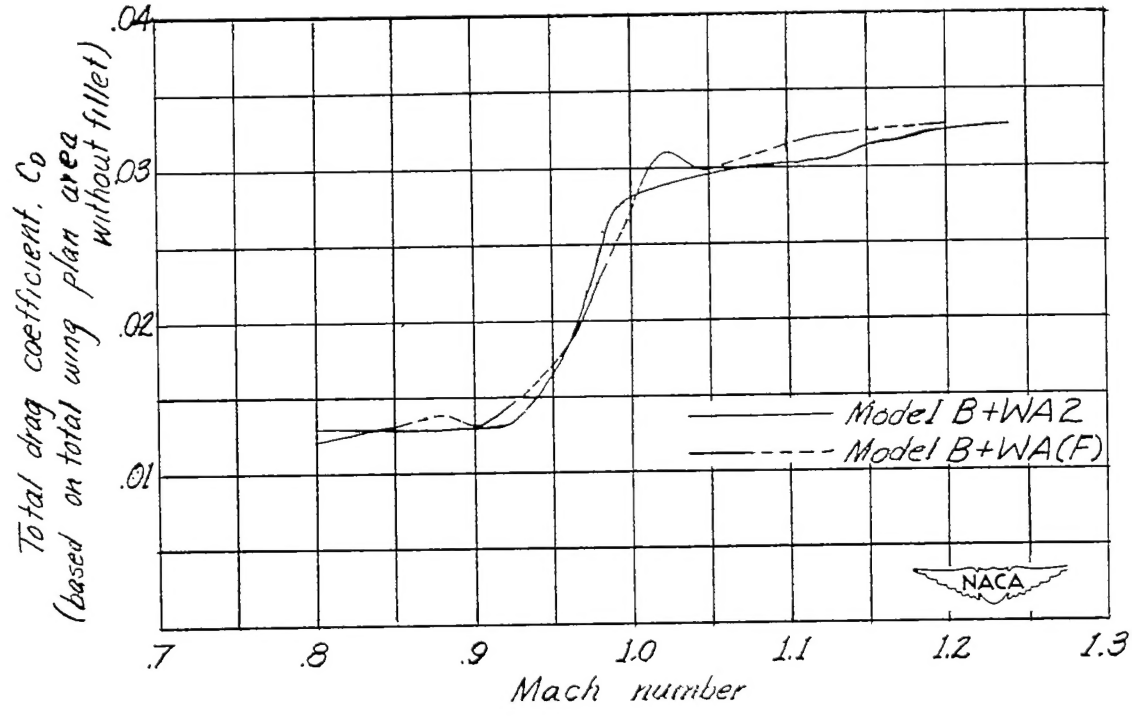

Figure 12.- Comparison of variations with Mach number of total drag coefficient for a wing-body combination with (model B + WA(F)) and without (model B + WA2) a large wing fillet.

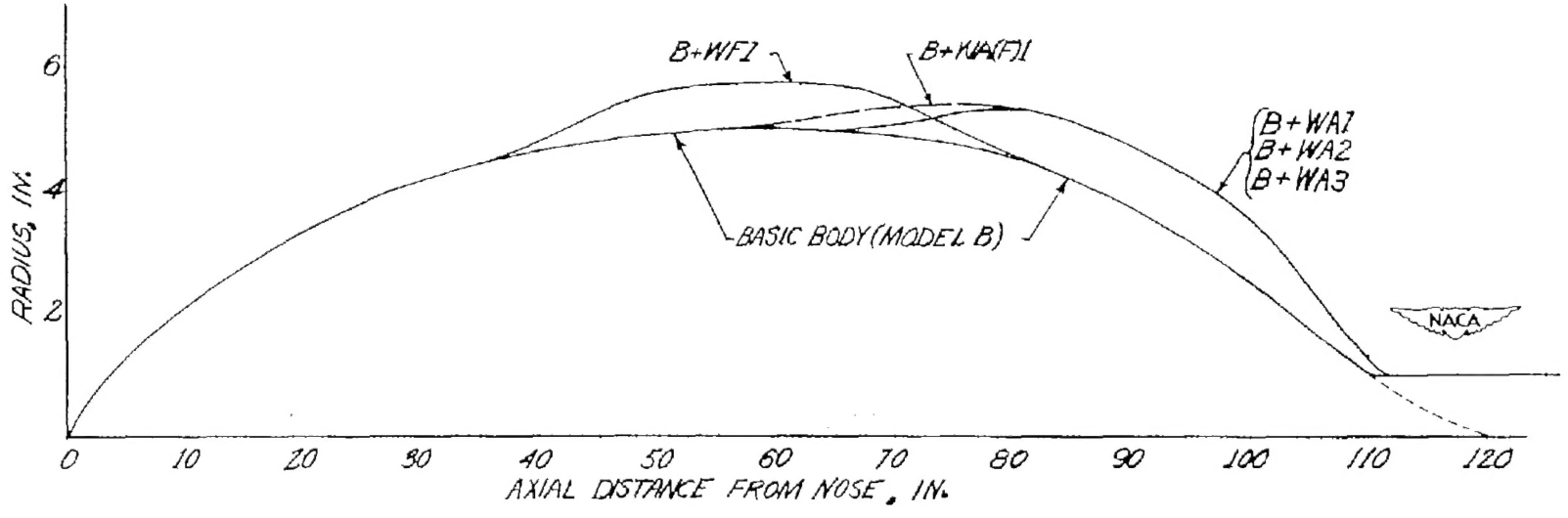

Figure 13.- Comparison of the shapes of bodies of revolution having the same axial distribution of cross-sectional area as wing-body configurations B + WA1, B + WA2, B + WA3, B + WF1, and B + WA(F) with the basic body shape (model B).